Carbon oxidation with sacrificial anodes to inhibit O_2 evolution in membrane-less bioelectrochemical systems for microbial electrosynthesis

*Nils Rohbohm[1], Tianran Sun[1,2], Ramiro Blasco-Gómez[1,3], James M. Byrne[4,5], Andreas Kappler[4,6] and Largus T. Angenent[1,6,7,8,9]**

* Corresponding author: Largus T. Angenent

[1] Environmental Biotechnology Group, Department of Geosciences, University of Tübingen, Schnarrenbergstr. 94-96, 72076 Tübingen, Germany

[2] State Key Lab of Urban and Regional Ecology, Research Center for Eco-Environmental Sciences, Chinese Academy of Sciences, Beijing 100085, China

[3] Laboratory of Chemical and Environmental Engineering (LEQUiA), Institute of the Environment, University of Girona, Carrer Maria Aurelia Capmany, 69, 17003 Girona, Spain

[4] Geomicrobiology, Department of Geosciences, University of Tübingen, Schnarrenbergstr. 94-96, 72076 Tübingen, Germany

[5] School of Earth Sciences, University of Bristol, Wills Memorial Building, Queens Road, Bristol, BS8 1RJ, United Kingdom

[6] Cluster of Excellence: EXC 2124: Controlling Microbes to Fight Infection, Tuebingen, 72076, Germany

[7] AG Angenent, Max Planck Institute for Biology, Max Planck Ring 5, D-72076 Tübingen, Germany

[8] Department of Biological and Chemical Engineering, Aarhus University, Universitetsbyen 36, 8000 Aarhus C, Denmark

[9] The Novo Nordisk Foundation CO_2 Research Center (CORC), Aarhus University, Gustav Wieds Vej 10, 8000 Aarhus C, Denmark

Contact information

E-mail: l.angenent@uni-tuebingen.de

Keywords

microbial electrosynthesis; oxygen inhibition; membrane-less, microbial electrochemical technology, carbon-assisted water electrolysis, carbon oxidation with sacrificial anodes

Abstract

Microbial electrosynthesis is an emerging biosynthesis technology that produces value-added chemicals and fuels and, at the same time, reduces the environmental carbon footprint. However, constraints, such as low current densities and high inner resistance, disfavor this technology for industrial-scale purposes. The cathode performance has been strongly improved in recent years, while the anode performance has not been given enough attention despite its importance in closing the electric circuit. For traditional water electrolysis, O_2 is produced at the anode, which is toxic to the anaerobic autotrophs that engage in microbial electrosynthesis. To overcome O_2 toxicity in conventional microbial electrosynthesis, the anode and the cathode chamber have been separated by an ion-exchange membrane to avoid contact between the microbes and O_2. However, ion-exchange membranes increase the maintenance costs and compromise the production efficiency by introducing an additional internal resistance. Furthermore, O_2 is inevitably transferred to the catholyte due to diffusion and electro-osmotic fluxes that occur within the membrane. Here, we proved the concept of integrating carbon oxidation with sacrificial anodes and microbes to simultaneously inhibit the O_2 evolution reaction (OER) and circumvent membrane application, which allows microbial electrosynthesis to proceed in a single chamber. The carbon-based anodes performed carbon oxidation as the alternative reaction to the OER. This enables microbial electrosynthesis to be performed with cell voltages as low as 1.8-2.1 V at 10 $A \cdot m^{-2}$. We utilized *Methanothermobacter thermoautotrophicus* ΔH in a single-chamber Bioelectrochemical system (BES) with the best performing carbon-based anode (*i.e.*, activated-carbon anode with soluble iron) to achieve a maximum cathode-geometric CH_4 production rate of 27.3 $L \cdot m^{-2} \cdot d^{-1}$, which is equal to a volumetric methane production rate of $1.1 \cdot 10^{-1}$ $L \cdot L^{-1} \cdot d^{-1}$ in our BES, at a coulombic efficiency of 99.4%. This proof-of-concept study allows microbial electrosynthesis to be

54 performed more energy-efficiently and can be immediately utilized for research purposes in the
55 microbial electrosynthesis field of study.
56
57 INTRODUCTION

58 Globally increasing demands for value-added chemicals and fuels require innovative chemical and
59 biochemical synthesis strategies to proceed in a more cost-efficient and environmentally friendly
60 manner. Microbial electrosynthesis is a bioprocess with bioelectrochemical systems to convert
61 inorganic gases into valuable, multi-carbon compounds to store excessive renewable energy such
62 as wind or solar energy (Nevin et al., 2010; Rabaey and Rozendal, 2010). This makes it an
63 attractive technology for achieving the goal of a carbon-neutral society. Microbial activity and
64 electrode performance are critical factors in determining the overall efficiency of microbial
65 electrosynthesis. However, the inherent problem of scaling-up microbial electrosynthesis is the
66 currently low current density of the bioelectrochemical system, which results in a considerably
67 lower production rate compared to chemical electrosynthesis that produces the same compounds
68 (**Table S1**). To increase the current density, the electrochemical performance must be increased
69 by, for example, improving the cathode performance. Indeed, several studies have focused on the
70 modification of the cathode to improve microbe-electrode interactions and its biocompatibility
71 (Tremblay et al., 2017; Kracke et al., 2020).

72 Besides the biocompatibility problems, another troublesome part of bioelectrochemical systems is
73 the ion-exchange membrane. Classically, the anode is separated from the cathode by an ion-
74 exchange membrane to avoid interaction of the O_2 evolving at the anode with the strict anaerobic
75 microbes in the cathodic chamber (Giddings et al., 2015). However, applying an ion-exchange
76 membrane in bioelectrochemical systems has several disadvantages. By including an ion-exchange

77 membrane, the internal resistance is increased (Długołęcki et al., 2010). This will lead to decreased
78 ion transport, which consequently limits electron transfer and reduces the current generation.
79 Ideally, protons are primarily transported from the anodic to the cathodic chamber to maintain
80 hydrogen production. However, the transfer of other cations, such as sodium or potassium, to the
81 cathode chamber cannot be neglected and reduces the ionic transport number of protons.
82 Consequently, the slower mass transfer rate of protons leads to a pH gradient (Rozendal et al.,
83 2006). In addition, the ion-exchange membrane also generates an electro-osmotic flow that allows
84 all ionic and non-ionic solutes, including O_2, to pass through the cathode chamber, thus, making
85 its purpose ineffective (Kim et al., 1996). The pore size of the membrane in addition to O_2
86 permeation, which allows biofilm formation, makes it vulnerable to fouling (Jourdin et al., 2018).
87 Finally, the capital costs for membranes are high, and combining all the other disadvantages will
88 result in high maintenance and operating costs (Fornero et al., 2010; Yee et al., 2012).

89 The ideal bioelectrochemical system would, therefore, be a single-chamber system in which the
90 ion-exchange membrane has been removed (Mano et al., 2004). This would improve not only the
91 current generation but also the synthesis efficiency. However, O_2 would still be produced without
92 modifications at the anode and hinder anaerobic microbes from growing for microbial
93 electrosynthesis to proceed. Thus far, few reports have been published showing membrane-less
94 bioelectrochemical systems, and most reports are about microbial fuel cells and enzymatic fuel
95 cells. Furthermore, most membrane-less, single-chamber systems were operated without O_2-
96 sensitive microbes (Call and Logan, 2008; Cheng et al., 2009). Giddings et al. (2015) designed a
97 membrane-less system for microbial electrosynthesis in which the anode was placed at the
98 boundary of the liquid interface to avoid O_2 from mixing. Besides, different patent applications for
99 single-chamber bioelectrochemical systems were filed with setups to capture and remove O_2 away

100 from the cathode (Lovley and Nevin, 2012; Kumar et al., 2020). However, none of these
101 innovations had tried to circumvent the O_2-evolution reaction (OER) at the anode.

102 An appealing approach to avoid O_2 formation at the anode is carbon-assisted water electrolysis
103 (CAWE) for which carbon is oxidized at the anode instead of the OER in conventional electrolysis
104 (Ju et al., 2018; Holubowitch et al., 2019). The classical hydrogen-evolution reaction (HER) is the
105 same for CAWE and conventional water electrolysis. CAWE can include: **(1)** the oxidation of
106 carbon-based electrodes, which we refer to as carbon oxidation with sacrificial anodes; and **(2)** the
107 oxidation of soluble carbon materials (which we did not study) or non-soluble carbon materials in
108 the anolyte. Here, we address carbon oxidation of sacrificial anodes, forming CO_2, CO, and
109 oxygenated surface-functional groups. The desired two chemical reactions can be described as
110 follows:

$$CO_2 + 4H^+ + 4e^- \rightarrow C + 2H_2O \qquad E^0 = +0.21\ V \quad (1)$$

$$CO + 2H^+ + 2e^- \rightarrow C + 2H_2O \qquad E^0 = +0.51\ V \quad (2)$$

111 A major advantage of using CAWE instead of conventional water electrolysis with O_2 evolution
112 at the anode is the lower operating cell voltage, resulting in lower energy consumption rates. For
113 example, the standard electrode cell potential for the four-electron process (**Eq. 1**) for CAWE is
114 $E^0_{cell,CAWE}$ = -0.21 V, while the conventional water electrolysis reaction requires $E^0_{cell,water}$
115 $_{electrolysis}$ = -1.23 V (Ju et al., 2018). Another advantage of CAWE compared to conventional water
116 electrolysis is the higher carbon-oxidation reaction rate than the OER rate at the anode (exchange
117 current density: $j_{0,CAWE} = 10^{-6}\ A \cdot cm^{-2}$ *vs.* $j_{0,OER} = 10^{-7}\ A \cdot cm^{-2}$) (Ju et al., 2018). Albeit, the carbon-
118 oxidation reaction at the anode is still slower than the HER rate at the cathode ($j_{0,HER} = 10^{-3}\ A \cdot cm^{-}$
119 ^{2}) (Carmo et al., 2013). Finally, a necessary substrate for microbial electrosynthesis is CO_2 or CO,

120 which is the desired product of carbon oxidation with sacrificial anodes. Thus, the matching
121 product formation as extra carbon source for the microbes is another pertinent advantage of carbon
122 oxidation with sacrificial anodes for microbial electrosynthesis.

123 An example of carbon oxidation with carbon-based anodes was shown by Holubowitch et al.
124 (2019), who demonstrated an abiotic membrane-less electrochemical cell that was capable of
125 reducing O_2 to deoxygenate water. While their main focus was on reducing O_2, we identified with
126 their data that either no O_2 was produced or O_2 production was decreased at the anode and that O_2
127 was electrochemically reduced at the cathode. Carbon oxidation with carbon-based anodes was
128 not only tested abiotically but also for bioelectrochemical systems. Lai et al. (2017) found a lower
129 O_2 content and a higher CO_2 content in their anodic compartment using graphite. They concluded
130 that carbon oxidation with the graphite anode was the main cause of the lower O_2 formation. A
131 follow-up study for the removal of perchloroethylene in a membrane-less bioelectrochemical
132 system used graphite granules as a single anode to avoid O_2 production (Zeppilli et al., 2019). To
133 our knowledge, carbon oxidation with sacrificial anodes has not been tested for microbial
134 electrosynthesis.

135 The objective of this work was a proof of concept to show that carbon oxidation can be utilized in
136 a single-chamber bioelectrochemical system to specifically perform microbial electrosynthesis.
137 We used different types of carbon electrodes as anodes and assessed whether O_2 formation was
138 inhibited or just decreased. In addition, we tested iron (soluble and coated) materials with carbon
139 electrodes to further circumvent the OER by including a parallel Faradaic reaction. After we had
140 studied the feasibility of our carbon electrodes and deciphered the mechanism of the inhibition,
141 we operated our carbon electrodes in bioelectrochemical systems to evaluate their potential for
142 microbial electrosynthesis. Here, we report the successful implementation of carbon oxidation with

143 a sacrificial anode for microbial electrosynthesis using *Methanothermobacter thermautotrophicus*
144 ΔH, which is an autotrophic and anaerobic microbe, and which is being used in the power-to-gas
145 concept to store renewable electric power into CH_4 gas (Martin et al., 2013).

146 **MATERIALS AND METHODS**

147 **Chemicals, strain, and medium**

148 All chemicals were used as received unless otherwise noted in the text. These chemicals were of
149 technical or analytical grade and were purchased from Sigma-Aldrich (St. Louis, USA), Alfa Aeser
150 (Haverhill, USA), Merck (Darmstadt, Germany), Thermo-Fischer (Waltham, USA), VWR
151 (Radnor, USA), and Carl Roth (Karlsruhe, Germany). The strain *M. thermautotrophicus* ΔH (DSM
152 1053) was obtained from the DSMZ (Braunschweig, Germany). A pre-culture was grown at 60°C
153 in 100-mL serum bottles with 20 mL of modified anaerobic MS-Medium (Fink et al., 2021)
154 containing (per liter): 6.77 g $NaHCO_3$; 0.17 g K_2HPO_4; 0.235 g $(NH_4)_2SO_4$; 0.09 g $MgSO_4$; 0.06
155 g $CaCl_2$ x 2 H_2O; 0.23 g KH_2PO_4; 1 mL trace elements (10x); 1 mL of 4 M H_2SO_4; 0.5 g L-cysteine
156 hydrochloride. The trace-element solution was a 10x stock solution containing (per 100 mL): 0.2
157 g nitrilotriacetic acid; 3 g $MgSO_4$ x 7 H_2O; 0.5 g $MnSO_4$; 0.3 g $FeSO_4$ x 7 H_2O; 0.11 g $CoSO_4$ x 7
158 H_2O; 0.068 g $CaCO_3$; 0.18 g $ZnSO_4$; 0.01 g $CuSO_4$ x 5 H_2O; 0.018 g $KAl(SO_4)_2$ x 12 H_2O; 0.01 g
159 H_3BO_3; 0.01 g Na_2MoO_4 x 2 H_2O; 0.48 g $(NH_4)_2Ni(SO_4)_2$ x 6 H_2O; 0.01 g Na_2WO_4 x 2 H_2O; 0.01
160 g Na_2SeO_4. The trace-element solution was adjusted to a pH value of 1 with H_2SO_4. The MS-
161 Medium was buffered only in the bioelectrochemical system by adding 2.5 M 3-(*N*-
162 morpholino)propanesulfonic acid (MOPS) at pH = 7.2 for a final media concentration of 25 mM.
163 All solutions were sterilized either through a sterile filter or autoclaved and made anaerobic by
164 sparging with N_2 or N_2/CO_2.

165 **Preparation of carbon-based electrodes**

166 The activated carbon served not only as active material but also as a conductive and surface
167 enlarging material and was used as purchased (~100 mesh particle size (~150 μm), DARCO®,
168 Cabot Norit Americas Inc, Marshall, USA). The activated carbon and paraffin oil (Sigma-Aldrich)
169 was homogeneously mixed in a mortar at 70%:30% to form a paste (Zhang et al., 2017). The
170 resulting paste was pelleted into a self-made electrode holder and cured in an 80°C vacuum oven
171 for 4 h. Activated-carbon-associated magnetite was synthesized through a co-precipitation method
172 by mixing activated carbon with 2 M $FeCl_3$ and 1 M $FeCl_2$ (Sorwat et al., 2020). Then, 20 %
173 NH_4OH was slowly dropped into the solution until pH 9. The solution was stirred for 1 h to
174 complete the synthesis of magnetite. The precipitate was centrifuged, cleaned with deionized water
175 until pH 7, and dried in a vacuum oven at 80°C for 4 h. Different amounts of activated carbon to
176 magnetite were used during the synthesis ranging from 0% to 60% of activated carbon. In this
177 study, activated carbon that was co-precipitated with magnetite is called magnetite-coated
178 activated carbon (**Supporting Information**). The 60% activated carbon and 40 % maghemite
179 mixture was synthesized by adding 60 % activated carbon and 40 % magnetite mixture into an
180 aerated oven at 80°C for 24 h.

181 **Measurement of dissolved O_2**

182 The O_2 measurements were carried out in a self-designed five-neck round flask. To measure the
183 dissolved O_2, an O_2-sensitive foil (0-100% O_2, PreSens Precision sensing, Regensburg, Germany)
184 was glued at the mid-height of the flask. The electrochemical cell was operated as a two-electrode
185 setup with a 1x1-cm carbon cloth electrode as the cathode. A platinum wire, a graphite rod, a
186 carbon cloth, activated carbon, and activated carbon that was coated with magnetite were used as

187 anodes. One experiment was performed with activated carbon as an anode with soluble iron. The
188 measurements were carried out in 0.066 M phosphate buffer at room temperature and 60°C. The
189 phosphate solution was buffered at 7.2 to mimic the pH of the MS medium used in the
190 bioelectrochemical system. Before each experiment, the cells were purged with N_2 gas for 1 h to
191 secure an O_2-free solution.

192 **Sample analyses**

193 The bioelectrochemical systems were sampled once per day. The gas compositions of the
194 bioelectrochemical systems were sampled with a 500-µL gastight syringe (Hamilton, Reno, USA)
195 and analyzed using a gas chromatograph (SRI GC, Torrance, USA). Coulombic efficiencies for
196 CH_4 were calculated according to Kracke et al. (2020). Cell growth was measured by cell counting
197 with a light microscope (X41, Olympus, Shinjuku, Japan). The anodes were collected after the
198 experiment and stored anoxically at -20°C for further analyses. The iron content from the liquid
199 samples and the oxidation state of iron in the magnetite electrodes were further analyzed *via* the
200 Ferrozine assay (Stookey, 1970; Sorwat et al., 2020).

201 **Electrochemical system**

202 All electrochemical measurements (cyclic voltammetry, linear sweep voltammetry, and
203 chronopotentiometry) were conducted in a five-neck round flask with a working volume of 50 mL.
204 The electrochemical cells were operated as a two-electrode or a three-electrode setup and
205 controlled *via* a potentiostat (VMP3, Bio-Logic, Grenoble, France). An Ag/AgCl (3M KCl, 0.210
206 V *vs*. SHE) in-house-made reference electrode was used for the three-electrode setup. All
207 measurements with a reference electrode were ohmic-drop corrected and were determined by
208 potentiostatic electrochemical-impedance spectroscopy. Ohmic-drop-corrected potentials were

209 calculated following the method of Sun et al. (2017). The reaction kinetics of carbon and magnetite
210 were calculated with the Butler-Volmer equation, using linear sweep voltammetry and cyclic
211 voltammetry measurements (Supporting Information). The 1x1-cm carbon cloth electrode
212 (PANEX 30-PW06, Zoltek, St. Louis, USA) and the platinum wire (Bioanalytical Systems, Inc.,
213 West Lafayette, USA) were used as cathodes, and the carbon-based electrode, graphite rod
214 (Mersen, Suhl, Germany), carbon cloth (Zoltek), the carbon paste electrode holder (Bio-Logic),
215 and the gold electrode (Bio-Logic) were used as anodes depending on their intended application,
216 which is described in the results part. The temperature was either room temperature or controlled
217 by a water bath at 60°C (ICC basic IB R RO 15 eco, IKA, Staufen im Breisgau, Germany). The
218 supporting electrolyte for the abiotic experiments was phosphate buffer (0.066 M) or phosphate
219 buffered saline (0.05 M), with the pH buffered at 7.2. Before each abiotic electrochemical
220 experiment, a high-purity N_2 gas was introduced to remove O_2. The bioelectrochemical systems
221 were either autoclaved or chemically sterilized before the beginning of each experiment. The
222 reactors were filled with 50-mL MS-Medium, were kept anaerobic by sparging with 80:20 (*v/v*)
223 N_2/CO_2 through a sterile filter, and were continuously stirred with a magnetic stir bar. The reactors
224 were operated in batch mode and were fed with pure CO_2 as the sole carbon source *prior* to the
225 experiment and every day after liquid sampling to exchange the headspace. The electrochemical
226 cells were submerged in a water bath to prevent heat loss for optimal growth of *M.*
227 *thermautotrophicus* ΔH at 60°C.

228 **Immobilization of magnetite**

229 Magnetite was immobilized by dispersing magnetite nanoparticles onto an Au electrode (Biologic)
230 to test its electrochemical behavior. The protocol is an adjusted version from Sun et al. (2017).
231 Briefly, ten milligrams of the active powder and 40 µL of Nafion were mixed with 960 µL 70%

232 ethanol and sonicated for 15 min. Then, 10 µL were drop casted onto the surface of the Au
233 electrode and dried at room temperature. To avoid iron from oxidizing, the preparations for the
234 drop casted magnetite were performed inside a glovebox (mBraun, Garching, Germany).

235 **SEM, EDX, X-ray diffraction, and FTIR**

236 A 50-µL aliquot of 0.1% poly-L-lysine solution was placed onto a glass slide and was dried for 1
237 h in a 60°C incubator. The samples were placed onto a poly-L-lysine coated glass slide that was
238 attached to aluminum stubs, using carbon adhesive tabs. The sample was coated with a 10-nm
239 deposition of platinum, using a BAL-TEC™ SCD 005 sputter coater (Leica biosystems, Nussloch,
240 Germany). The purpose of the coating was to reduce any charging effects during scanning electron
241 microscope (SEM) analysis. All images were taken in secondary-electron (SE) mode using a Zeiss
242 Crossbeam 550L focused ion beam (FIB) SEM (Zeiss, Wetzlar, Germany), which was operated
243 with an acceleration voltage of 2 kV. The SEM was equipped with an Oxford Instrument energy
244 dispersive spectrometry detector (Ultim Max, Oxford Instrument, Abingdon, United Kingdom).
245 Elemental maps of iron and carbon were obtained along with corresponding spot analysis.

246 X-ray diffraction (XRD) was carried out on dry material using Bruker's D8 Discover GADDS
247 XRD2 micro-diffractometer that was equipped with a Co-anode (Cu Kα radiation, $\lambda = 0.154$ nm)
248 at parameters of 30 kV/30mA (Billerica, USA). The total measurement time was 240 s at two
249 detector positions, which were 15° and 40°. Fourier transform infrared (FTIR) spectroscopy was
250 performed on a Vertex 80v equipped with an RT-DLaTGS detector (Bruker, Billerica, USA). 0.5
251 mg of sample was mixed homogenously with 250 mg KBr (FTIR grade, Carl Roth, Karlsruhe,
252 Germany) and compressed at 10T to form a pellet. Samples were scanned 32 times in the range of
253 400-4500 cm^{-1}.

RESULTS

Electrochemical characterization of carbon oxidation and O_2 evolution for CAWE and conventional water electrolysis

For our proof-of-concept process, we used the two carbon-oxidation reactions from CAWE compared to the OER from conventional water electrolysis. The two carbon-oxidation reactions have a theoretically more favorable thermodynamic potential of +0.21 V *vs.* RHE for CO_2 production (four electrons in **Eq. 1**) and +0.51 V *vs.* RHE for CO production (two electrons in **Eq. 2)**, respectively, than the OER, with a standard potential of +1.23 V *vs.* RHE. For conventional water electrolysis with the OER, the overall cell potential would be -1.23 V. However, electrode materials have properties that introduce an overpotential. In the case of carbon electrodes, the overpotential can be up to 500 mV or higher (Yi et al., 2017).

To measure the overpotentials (η) for our specific system for carbon oxidation with carbon-based anodes, OER, and HER, we performed linear sweep voltammetry on the activated carbon (as the anode) and carbon cloth (as the cathode). Linear sweep voltammograms demonstrated that the measured overpotential ($|\eta| = [E_{onset\ potential} + E_{reference\ electrode\ correction}] - [E^0 - 0.059 \cdot pH]$) of carbon oxidation with activated carbon was +1.16 V, while the HER for carbon cloth had an overpotential of +0.190 V (**Fig. 1**). Thus, the minimum required cell potential for CAWE anodes would be -1.56 V ($E^0_{HER} - \eta_{HER} - [E^0_{carbon\ oxdiation} + \eta_{carbon\ oxidation}]$), which is -1.37 V lower than the theoretical value ($E^0_{cell,\ carbon\ oxidation} = E^0_{HER} - E^0_{carbon\ oxidation} = -0.21$ V). The OER with the activated carbon had an overpotential of +0.86 V (**Fig. 1**). Therefore, the minimal required cell potential for conventional water electrolysis would be equivalent to -2.28 V ($E_{cell,\ water\ electrolysis} = E^0_{HER} - \eta_{HER} - [E^0_{OER} + \eta_{OER}]$), which is -1.05 V lower than the theoretical value. The considerably higher systems

potential for CAWE compared to conventional water electrolysis should lower the energy consumption in our system as well.

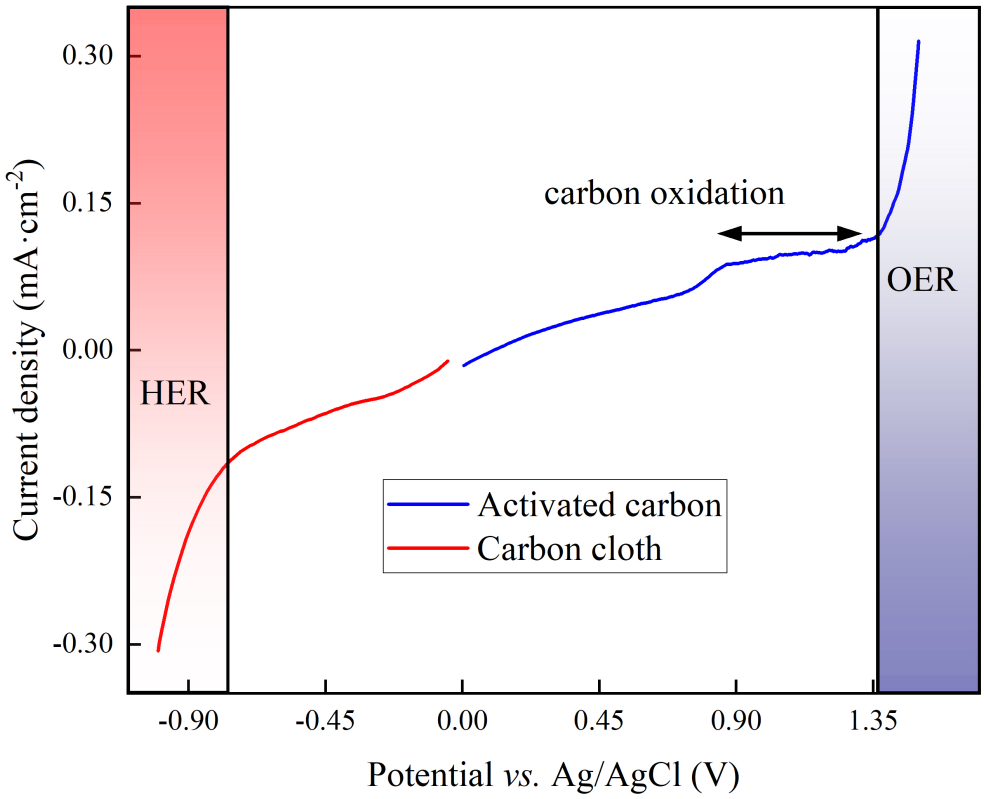

Figure 1: Linear sweep voltammogram of the activated-carbon anode (blue line) and the carbon-cloth cathode (red line) in 66 mM phosphate buffer (pH = 7.2) at a scan rate of 20 $mV \cdot s^{-1}$.

However, besides the cell potentials, the kinetics of the different electrochemical reactions are also important. The linear-sweep voltammogram of activated carbon did not show any pristine carbon-oxidation peaks to compare the kinetic value of the carbon oxidation to the OER (**Fig. 1**). However, the exchange current density, which is a dimension of the reaction rate, can be deduced from the linear-sweep voltammograms by means of the Butler-Volmer equation (Supporting Information) (Bard and Faulkner, 2000). The exchange current density for carbon oxidation was 10^{-5} $A \cdot cm^{-2}$

287 and was one magnitude higher than the OER at 10^{-6} A·cm^{-2}. Therefore, the carbon oxidation
288 reaction with sacrificial anodes is a faster electrochemical reaction than OER.

289 **Carbon-based anodes circumvent the need for a membrane**

290 To identify whether O_2 production is inhibited or decreased, we measured the O_2 content of an
291 abiotic, two-electrode electrochemical system for five days. This experiment was performed in
292 triplicate for two temperature conditions: room temperature and 60°C. We used a graphite rod,
293 carbon cloth, and activated carbon as our carbon anodes for five treatments and included a platinum
294 anode that was poised at 10 A·m^{-2} in 0.066 M phosphate buffer as the positive control to compare
295 the results of the carbon oxidation with sacrificial anodes to the OER (**Fig. 2**). All carbon-based
296 anodes showed an inhibitory effect on the O_2 production compared to the positive control for the
297 first 180 min at room temperature, with the graphite-rod and carbon-cloth anodes producing more
298 O_2 compared to the activated-carbon anodes (**Fig. 2A**). We turned off the electrochemical system
299 with the platinum anode after 180 min to avoid accumulating O_2 and H_2 and creating a Knallgas
300 reaction. While the accumulated O_2 concentration of all the carbon-based anodes was relatively
301 low (<1 ppm), only the activated-carbon anode could sustain a nearly O_2-free environment after
302 five days (**Fig. 2B**).

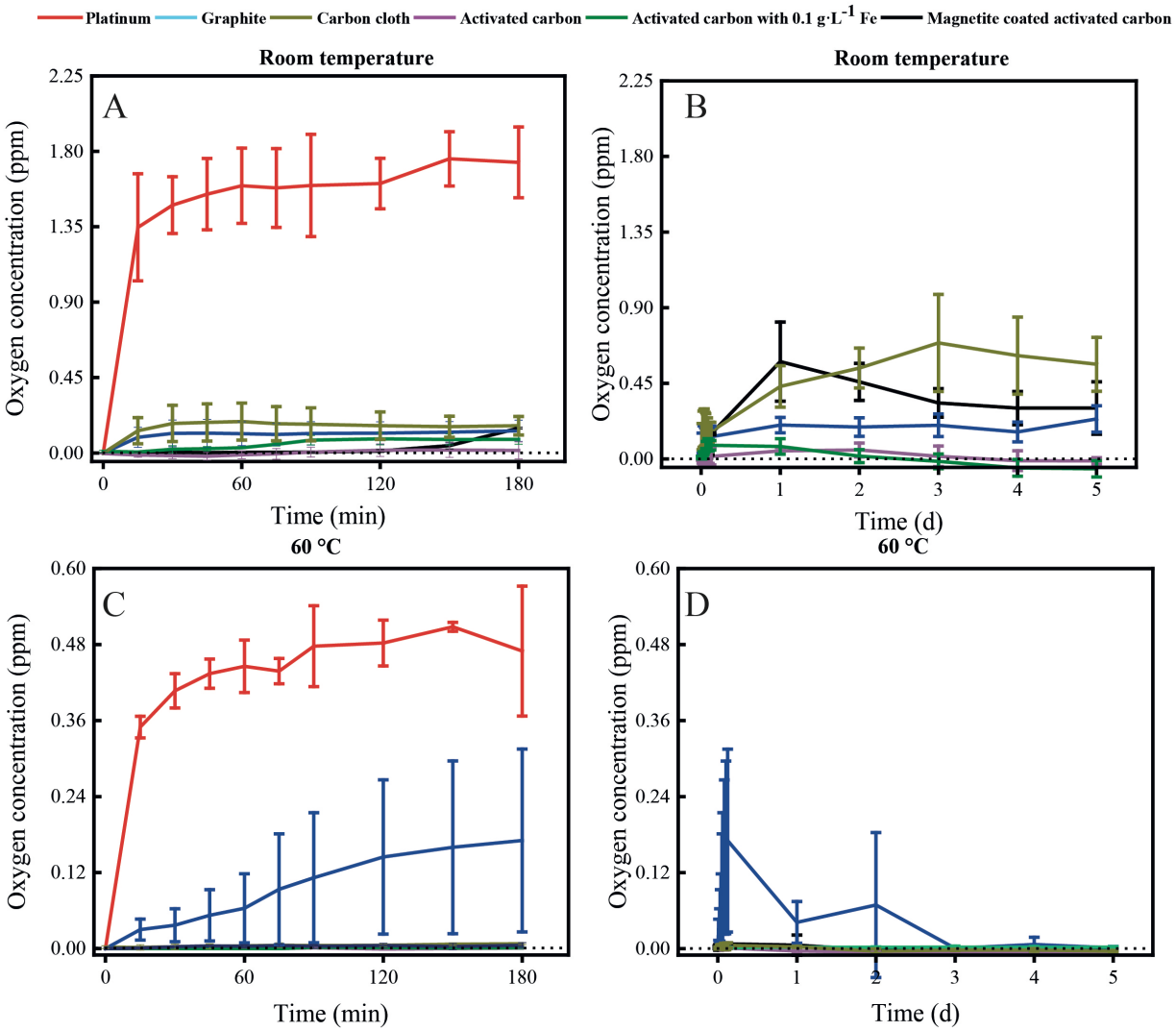

Figure 2: O_2 concentration in the electrolyte of platinum, graphite-rod, carbon-cloth, and activated-carbon anodes over time. Two temperature conditions were included. Three treatments with activated carbon were included, including iron additions. The error bars show the standard deviation for the average date from triplicate systems: **(A)** the O_2 concentration at room temperature for 180 min; **(B)** the O_2 concentration at room temperature for 5 days; **(C)** the O_2 concentration at 60°C for 180 min; and **(D)** the O_2 concentration at 60°C for 5 days. We omitted the data for the first 180 min from panels B and D for clarity reasons.

In contrast, all the experiments with carbon-based anodes at 60°C inhibited O_2 production after 180 min, except for the graphite-rod anode (**Fig. 2C**). Since the kinetics of a reaction are directly related to the temperature, an increase in the temperature will, therefore, increase the carbon-oxidation rate. Subsequently, a faster carbon-oxidation rate will reduce or inhibit the OER. After five days, the O_2 concentration in the electrolyte with the graphite-rod anode gradually decreased, suggesting that graphite needs an activation time to oxidize its surface and efficiently perform

315 carbon oxidation (**Fig. 2D**). The concentrations of CO_2 and CO were measured for the two
316 temperature conditions and the five treatments. The concentrations were very low for both gases
317 due to the low applied current and were not further monitored. In summary, the carbon-based
318 anodes circumvented O_2 production at 60°C and were used for further thermophilic BES
319 experiments.

320 **Carbon-based anodes in single-chamber bioelectrochemical systems for microbial**
321 **electrosynthesis**

322 In our proof-of-concept BES for microbial electrosynthesis, we opted for the microbe *M.*
323 *thermautotrophicus* ΔH due to its high growth rate (doubling time of 120 min) and relatively high
324 CH_4 production rate (Martin et al., 2013). This archaeal strain grows anoxically at 60°C and shows
325 a resilient behavior in the presence of O_2 by having the ability to grow after exposure to air for
326 several hours (Kiener and Leisinger, 1983). However, as a strict anaerobic methanogen, it is still
327 sensitive to O_2 for longer operating periods, resulting in the absence of growth when prolonged O_2
328 is present. The BES experiments were performed at 60°C and close to neutral-pH conditions with
329 graphite-rod and activated-carbon anodes in an experimental design with four treatments (**Fig. 3**).

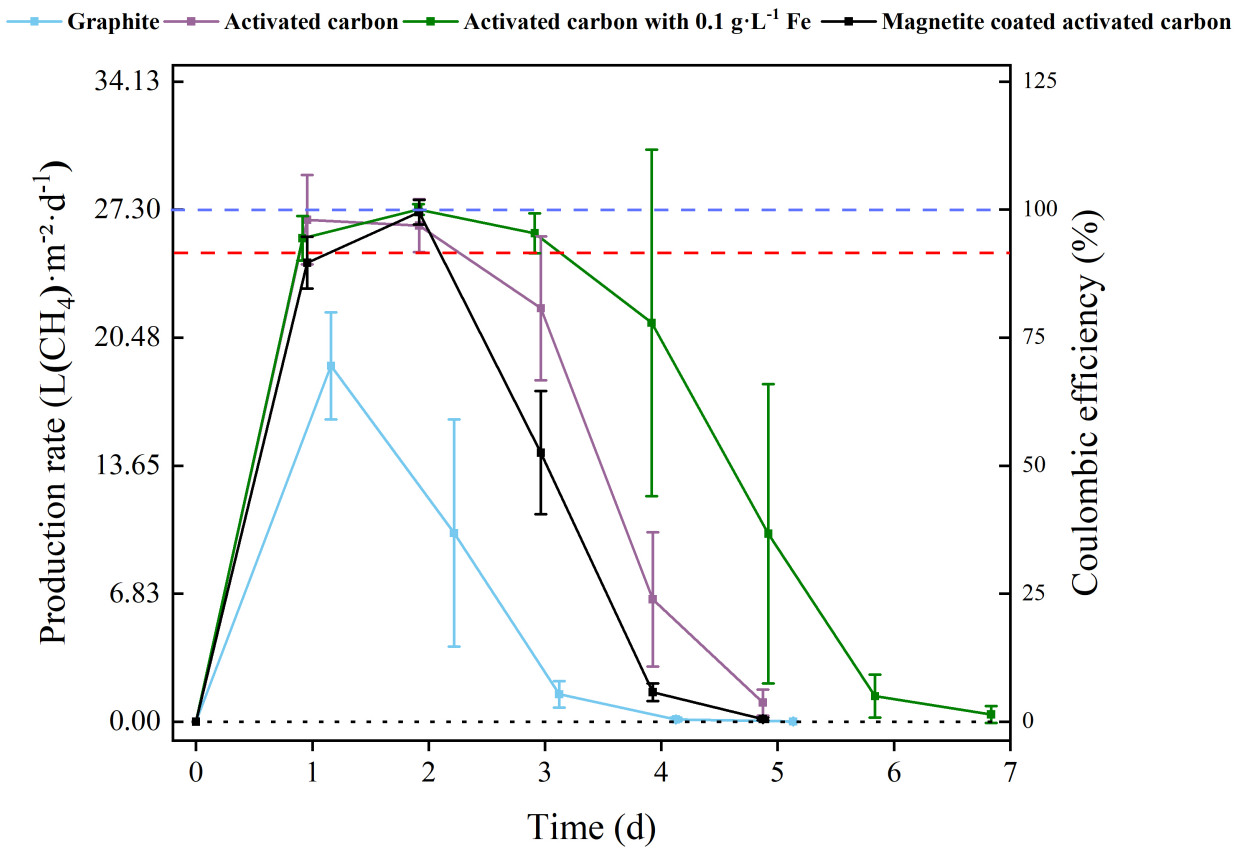

Figure 3: CH_4 production rates corrected to the cathode surface area and Coulombic efficiencies (at I = 10 $A \cdot m^{-2}$) during batch experiments over time with the thermophilic archaeon *M. thermautotrophicus* ΔH. Graphite-rod and activated-carbon anodes were included with three treatments for activated carbon, including iron additions (soluble iron and magnetite). The error bars show the standard deviation for the average data from triplicate systems. Carbon cloth was used as the cathode: **(**Y-axis 1) cathode-based geometric CH_4 production rates for four treatments; and **(**Y-axis 2**)** Coulombic efficiencies for four treatments. While the blue-dotted line represents 100% Coulombic efficiency, the red-dotted line shows the empirical cathode-based geometric CH_4 production rate of > 25 $L \cdot m^{-2} \cdot d^{-1}$ to determine the duration of the optimum performance period.

M. thermautotrophicus ΔH produced CH_4 with CO_2 as the sole carbon source during carbon oxidation with sacrificial anodes for all treatments (**Fig. 3**). After an operating period of one day, the maximum cathode-based geometric CH_4 production rates for the BESs with the graphite-rod and activated-carbon anode were 18.97 and 26.75 $L \cdot m^{-2} \cdot d^{-1}$, respectively. This resulted in a maximum volumetric CH_4 production rate of 0.1 $L \cdot L^{-1} \cdot d^{-1}$ for the BES with the activated-carbon anode. Coulombic efficiencies of 97.96 % for the BES with the activated-carbon anodes suggest an efficient H_2 uptake by the microbes at the cathode (**Fig. 3)**.

345 To compare the different experimental conditions in our study, we choose an empirical cathode-
346 based geometric CH_4 production rate of > 25 $L \cdot m^{-2} \cdot d^{-1}$ to determine the duration of the optimum
347 performance period for each treatment. Under this definition of the optimum performance period,
348 the graphite-rod anode never reached this CH_4 production rate, resulting in an optimum
349 performance period of zero (**Table 1**) because the cathode-based geometric CH_4 production rate
350 was only 18.97 ± 2.84 $L \cdot m^{-2} \cdot d^{-1}$ on Day 1 of the operating period (**Fig. 3**). On the other hand, after
351 an operating period of two days, the cathode-based geometric CH_4 production rates for the BESs
352 with the activated-carbon anode was 26.44 ± 1.40 $L \cdot m^{-2} \cdot d^{-1}$ after which it decreased, resulting in
353 an optimum performance period of two days (**Table 1**). Thus, we were only able to maintain the
354 CH_4 production rate for the BES with activated-carbon anodes during an operating period of two
355 days. For all experimental conditions, the pH remained constant at 7.5, and CO_2 was never limited.

Table 1 | Performance data of the carbon-based anodes and its limiting factor.

Carbon-based anode	**Maximum geometric CH_4 production rate in $L \cdot m^{-2} \cdot d^{-1}$**	**Maximum volumetric CH_4 production rate in $L \cdot L^{-1} \cdot d^{-1}$**	**Optimum performance period in d**	**Limiting factor**
Graphite	18.97	0.07	0	Strong carbon structure
Activated carbon	26.75	0.10	2	Carbon availability
Activated carbon with 0.1 $g \cdot L^{-1}$ of Fe^{2+}	27.30	0.11	3	Carbon availability
Magnetite-coated activated carbon	27.15	0.11	2	Carbon availability

Our abiotic O_2 measurements with graphite-rod anodes (see the previous section) showed O_2 production, explaining that O_2 inhibition to the methanogen was the reason for the lower and faster diminishing CH_4 production during our BES experiment with graphite-rod anodes compared to the activated-carbon anodes. However, the activated-carbon anodes during abiotic experiments exhibited no O_2 production after an operating period of five days. The diminishing optimum CH_4 production during our BES experiment with activated-carbon anodes after two days was, therefore, not O_2 production but rather the oxidation and the removal of the carbon anode itself, sacrificing proper operating conditions due to a lack of accessible carbon. Thus, future BESs need to be packed with carbon-based anode material to lengthen the optimum performance period. Our proof-of-concept systems used relatively small geometric anode surfaces of 1.57 cm^2.

Ideally, we have the carbon oxidation donating four electrons and producing CO_2 (**Eq. 1**). To calculate the radius change (Δr) during the two-day optimum performance period of the activated carbon anode, we first calculated the volume of carbon that was consumed (**Eqs. 3-6**), which was equivalent to $1.10 \cdot 10^{-2}$ cm^3 ($8.95 \cdot 10^{-4}$ mol carbon) using the equation of the Coulombic efficiency (Kracke et al., 2020). The exposed surface of the activated carbon anode corresponded to a halved cylinder so that the volume after the optimum performance period and its corresponding radius change are:

$$V_{after\ optimum\ performance} = V_{start} - V_{consumed} = \frac{1}{2} \cdot \pi \cdot {r_{start}}^2 h - 1.10 \cdot 10^{-2}\ cm^3 \tag{3}$$

$$\frac{1}{2} \cdot \pi {r_{after\ optimum\ performance}}^2 h = V_{start} - V_{consumed} \tag{4}$$

$$r_{after\ optimum\ performance} = \sqrt[2]{\frac{(V_{start} - V_{consumed}) \cdot 2}{\pi \cdot h}} \quad (5)$$

$$\Delta r = r_{start} - r_{after\ optimum\ performance} \approx 34\ \mu m \quad (6)$$

With r_{start} = 0.475 cm and h = 2.175 cm. The relatively small change in the radius of 34 µm shows that the performance of the system was limited by the accessible carbon due to the low surface area.

We achieved a maximum cathode-based geometric CH_4 production rate of 26.75 $L \cdot m^{-2} \cdot d^{-1}$, which was identical to Kracke et al. (2020), who achieved a maximum of 26.76 $L \cdot m^{-2} \cdot d^{-1}$. The authors utilized a mesophilic methanogen (*i.e.*, *Methanococcus maripaludis*) in a BES with membranes and a NiMo cathode. However, the reported maximum volumetric CH_4 production rate by Kracke et al. (2020) was 1.38 $L \cdot L^{-1} \cdot d^{-1}$, which was 14 times higher than the 0.1 $L \cdot L^{-1} \cdot d^{-1}$ for our study due to a more optimum electrode-surface-to-reactor-volume ratio. An even higher volumetric CH_4 production rate as Kracke et al. (2020) was achieved by Baek et al. (2022) of 2.9 ± 1.2 $L \cdot L^{-1} \cdot d^{-1}$ using a zero-gap electrochemical cell. Despite its lower geometric CH_4 production rate of 18.25 $L \cdot m^{-2} \cdot d^{-1}$ and side-products of acetate and propionate, the zero-gap electrochemical has an optimized electrode-surface-to-reactor-volume ratio and has the potential to increase the production rates for microbial electrosynthesis, including for our system. Noteworthy is the considerably lower volumetric CH_4 production rates for all BES studies when compared to gas fermentation by sparging H_2 and CO_2 for which volumetric methane production rates of 163 $L \cdot L^{-1} \cdot d^{-1}$ had already been achieved in the 1990s (Schill et al., 1996). It is clear that several breakthroughs are necessary to close the gap between microbial electrosynthesis and gas fermentation for CH_4 production.

392 **Dissolved iron for increased current densities and CH_4 production rates**

393 Carbon oxidation with sacrificial anodes is still a relatively slow electrochemical reaction
394 compared to HER, even though the reaction rate is higher than OER (see exchange current density
395 from the previous section). Studies with abiotic electrochemical systems have shown that the
396 current density for carbon oxidation with sacrificial anodes can be increased by adding a soluble
397 redox mediator, such as Fe^{2+}, without reducing the Coulombic efficiency (Yin et al., 2009). Soluble
398 Fe^{2+} is directly reduced at the carbon-based anode to Fe^{3+} at electrochemical rates that are higher
399 than carbon oxidation and the OER (**Eq. 7** and **Fig. 4**). Therefore, soluble Fe^{2+} is an ultimate
400 electron donor in addition to the carbon-based anodes when Fe^{2+} is continuously added to the
401 system. However, even without continuous soluble Fe^{2+} addition, a current increase can be
402 anticipated due to the circular nature of the electron-mediating process, with the ultimate electron
403 donor coming from the carbon-based anode material than the continuously added Fe^{2+}. This is due
404 to indirect carbon oxidation by Fe^{3+} using carbon in the solution that originated from carbon
405 corrosion at the anode (**Fig. 4**). Carbon corrosion will be discussed in a later section. Indirect
406 carbon oxidation reduces Fe^{3+} back to Fe^{2+} in solution, while carbon is oxidized to CO_2 (**Eq. 8** and
407 **Fig. 4**). The reactions of the electron-mediating process can be described as follows:

At the anode: $\mathrm{Fe^{3+} + e^- \rightarrow Fe^{2+}}$ (7)

In the electrolyte: $\mathrm{C + 4Fe^{3+} + 2H_2O \rightarrow CO_2 + 4Fe^{2+} + 4H^+}$ (8)

408 Because the reduction and oxidation of soluble iron species occur at the anode and with carbon in
409 solution in the electrolyte, respectively, there is a continuous reformation of Fe^{2+} to maintain a
410 higher current density for the electrochemical cell. An advantage of the circular nature of this
411 electron-mediating process is that Fe^{3+} is oxidized in the electrolyte with carbon and not at the

cathode, which, as a competing process, would have reduced the Coulombic efficiency for methane production.

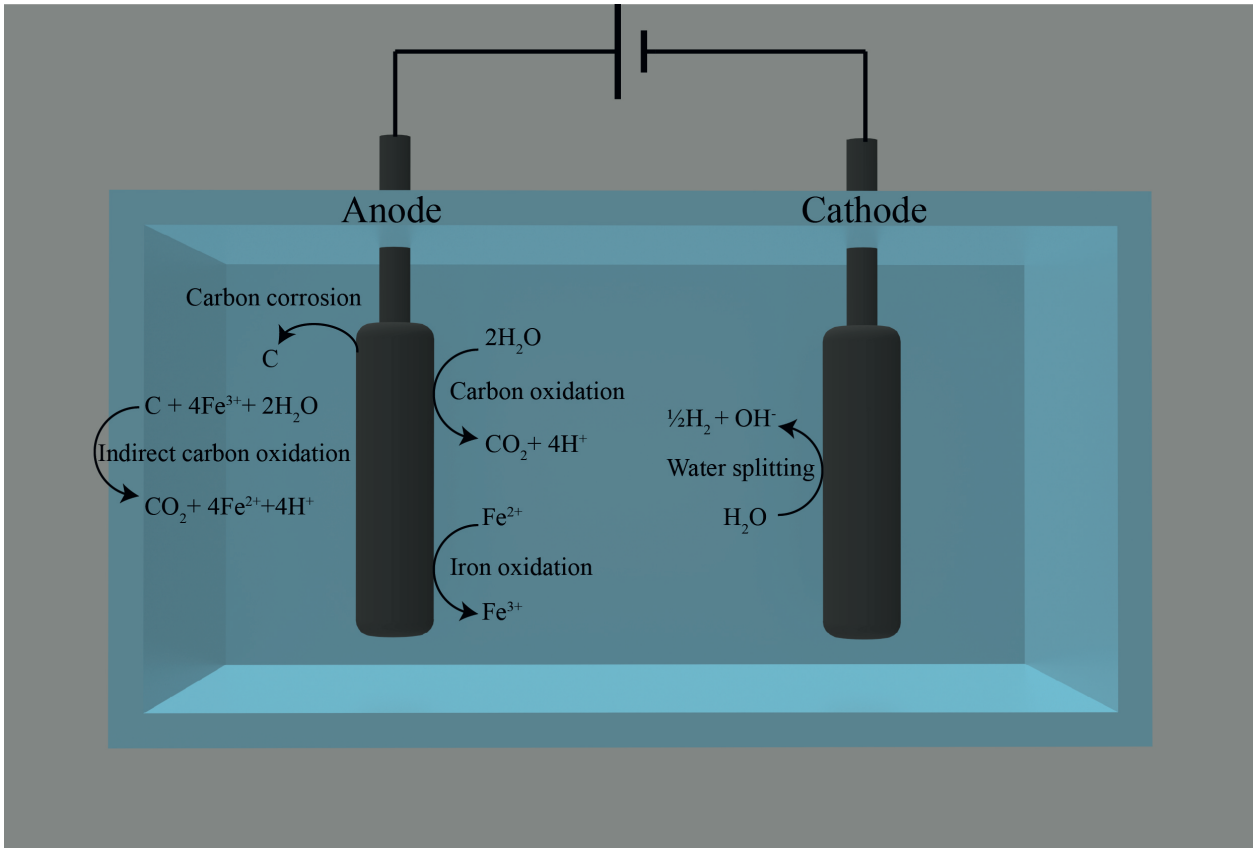

Figure 4: Overview of the reactions that occur at the anode and cathode during the carbon oxidation using activated carbon anodes with 0.1 $g \cdot L^{-1}$ of Fe^{2+}. Water splitting takes place at the cathode to produce H_2. The main reaction at the anode is carbon oxidation followed by the oxidation of Fe^{2+} and indirect carbon oxidation by the formed Fe^{3+}. For more information, see section dissolved iron for increased current densities and CH_4 production rates.

Before we tested BESs with soluble iron, we tested abiotically whether O_2 would be produced with activated-carbon anodes and 0.1 $g \cdot L^{-1}$ of Fe^{2+} (corresponding to 0.27 $g \cdot L^{-1}$ $FeSO_4$). As anticipated, no O_2 was produced at 60°C (**Fig. 2D**). Next, we tested whether a higher methane production rate was possible by adding Fe^{2+} to activated-carbon anodes without reducing the Coulombic efficiency, which we predicted based on abiotic work from others (**Fig. 3**). We performed the same BES experiment at 60°C with *M. thermautotrophicus* ΔH and activated-carbon anodes, except that we added 0.1 $g \cdot L^{-1}$ Fe^{2+}. We achieved a higher maximum cathode-based geometric CH_4 production

426 rate of 27.30 $L \cdot m^{-2} \cdot d^{-1}$, resulting in a volumetric CH_4 production rate of 0.11 $L \cdot L^{-1} \cdot d^{-1}$ and a higher
427 Coulombic efficiency of 99.36% with the added soluble iron than without (**Table 1**, **Fig. 3)**. In
428 addition, the optimum performance period was three days at an average cathode-based geometric
429 CH_4 production rate of 25.09 ± 2.94 $L \cdot m^{-2} \cdot d^{-1}$ with soluble iron rather than two days without
430 soluble iron addition. Thus, the addition of soluble iron to activated-carbon anodes as sacrificial
431 anodes for carbon oxidation increased the CH_4 production rates while maintaining an almost 100%
432 Coulombic efficiency, verifying our prediction.

433 Because we utilized the same amount of activated-carbon anode material for the experimental run
434 with and without soluble Fe^{2+}, both the added soluble Fe^{2+} and the soluble carbon from carbon
435 corrosion acted as additional ultimate electron donors to explain the increase in CH_4 production
436 rate. However, the system was still limited by the amount of accessible carbon-based anode
437 material, explaining the drop in performance after Day 3 of the operating period (**Fig. 3**). More
438 than four protons (**Eq. 1** and **Eq. 8**) and only two hydroxyl ions (HER) were produced per two
439 transferred electrons (**Fig. 4**), generating more net protons. However, we did not observe a decrease
440 in pH in our BES throughout the operating period because of the buffering capacity of the MOPS
441 and the produced CO_2 (**Fig. S7**).

442 **Magnetite as an alternative redox mediator to soluble iron shortened the optimum**
443 **performance period.**

444 Because the addition of soluble Fe^{2+} to activated-carbon anodes improved CH_4 production in our
445 microbial electrochemical system, we assessed whether an iron mineral would have a similar
446 positive effect. This iron mineral needed to: **(1)** be non-toxic for microbes; **(2)** have a faster redox
447 reaction than both the carbon oxidation and the OER; and **(3)** be conductive so that the current

generation would not be harmed. We opted for magnetite, which we produced as described in the material methods and analyzed (**Supporting Information**). For our BES experiments, we coated the magnetite on our activated-carbon anode. Magnetite is a mixed-valent Fe(II),Fe(III) magnetic iron mineral that oxidizes to maghemite (γ-Fe_2O_3), donating one electron (**Eq. 9**):

$$4\,\gamma - Fe_2O_3 + Fe^{2+} + 2e^- \rightarrow 3Fe_3O_4 \tag{9}$$

The cyclic voltammogram of synthesized magnetite nanoparticles that were immobilized on an Au electrode featured two peaks with a peak splitting of +0.28 V, representing the oxidative peak at -0.12 V *vs.* Ag/AgCl and the reductive peak at -0.41 V *vs.* Ag/AgCl (**Fig. 5A**). The comparison of the standard potential of both magnetite-oxidation reactions with the literature exhibited that the two-electron oxidation of magnetite to maghemite (**Eq. 9**) occurred for our system (Bradley and Tratnyek, 2019). The two electrons for magnetite oxidation compared to the four electrons for the

primary carbon oxidation reaction (**Eq. 1**) and the four electrons for OER, would reduce the anodic reaction potential considerably, which would be an advantage for using magnetite.

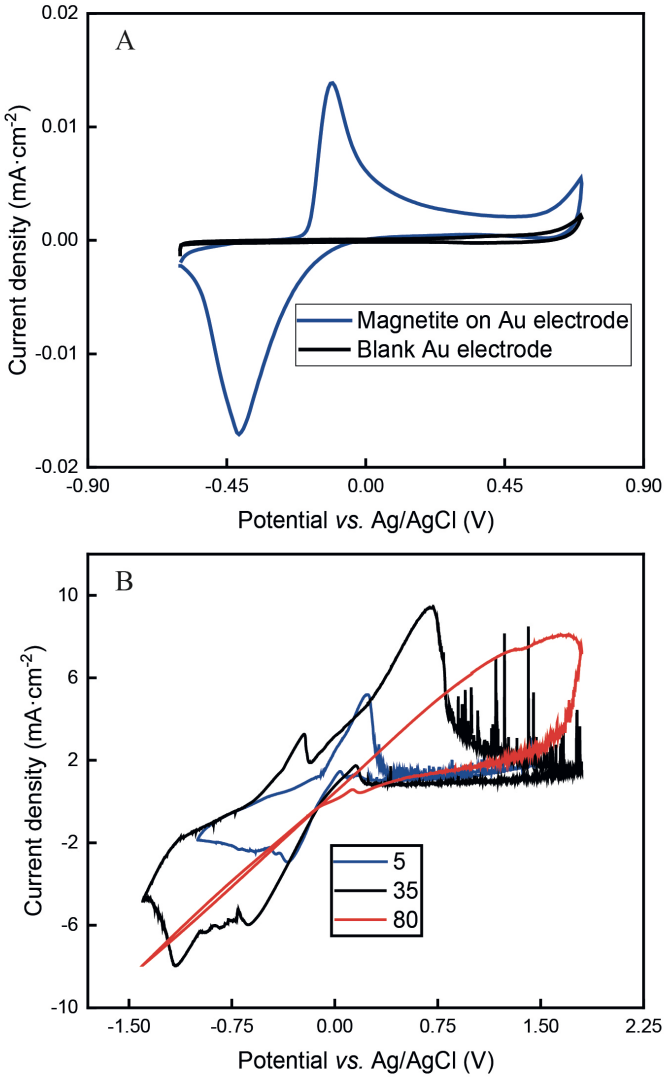

Figure 5: Electrochemical analysis of magnetite: **(A)** cyclic voltammogram of magnetite nanoparticles that were drop-casted on an Au electrode at a scan rate of 20 mVs^{-1} in 66 mM phosphate buffer. **(B)** cyclic voltammograms of bulk magnetite at cycle 5, 35, and 80 at a scan rate of 20 mVs^{-1} in 50 mM PBS.

The abiotic O_2 measurements of magnetite-coated activated-carbon anodes showed a higher O_2 concentration at room temperature compared to the other activated carbon-based electrodes (**Fig. 2**). However, the abiotic O_2 measurement at 60°C showed no O_2 production for a period of 5 days

467 similar to the other activated-carbon anodes (**Fig. 2C** and **D**), which would allow magnetite-coated
468 activated-carbon anodes to function in our BESs with *M. thermautotrophicus* ΔH. Therefore, we
469 performed the same BES experiments compared to activated-carbon anodes, except that we
470 applied magnetite to the activated-carbon anode material. The average cathode-based geometric
471 CH_4 production rate during the first two days was 25.80 ± 1.01 $L \cdot m^{-2} \cdot d^{-1}$ with an average
472 Coulombic efficiency of 93.97 ± 3.12% (**Fig. 3)**. After three days, the CH_4 production rate halved
473 and then dropped further to zero after four days (**Fig. 3)**. Therefore, the optimum performance
474 period was only two days, which is one day shorter than for the activated-carbon anodes with
475 soluble Fe^{2+} and identical for the activated-carbon anodes without soluble Fe^{2+} (**Table 1**). Finally,
476 the maximum cathode-based geometric CH_4 production rate for magnetite-coated activated-carbon
477 anodes of 27.15 $L \cdot m^{-2} \cdot d^{-1}$ was similar to the 27.30 $L \cdot m^{-2} \cdot d^{-1}$ for activated-carbon anodes with
478 soluble iron. However, compared to soluble iron, magnetite had a considerably lower impact as a
479 redox mediator.

480 The reduced amount of accessible activated-carbon anode material for carbon oxidation explains
481 the shorter optimum performance period of two days *vs*. three days for magnetite-coated anodes
482 and activated-carbon anodes, respectively. While the overall weight of the magnetite-coated
483 activated carbon material was kept equal to the other activated-carbon anodes, it consisted of 40%
484 less activated carbon, which in this system would be the ultimate electron donor. Possibly, this
485 experiment would have shown a more positive outcome with a much lower amount of magnetite,
486 showing the electron mediating activity of magnetite. However, there is a problem with magnetite

487 that would be difficult to overcome, making magnetite a less likely candidate for improved
488 performance than soluble iron.

489 Roberts et al. (2014) had shown that magnetite is prone to develop an irreversible reaction, which
490 would have a negative impact on long-duration BES experiments. Indeed, the cyclic
491 voltammograms of bulk magnetite showed decreasing reaction rates with increasing cycles (**Fig.**
492 **5B**), which can be explained by the formation of maghemite (**Eq. 9**). To quantify the reaction rates,
493 Tafel slopes were calculated from bulk magnetite during different cycles of the cyclic
494 voltammogram (Supporting Information note 1 and **Fig. 5B**). Bulk magnetite electrodes achieved
495 187 mV/dec at cycle 5 and transitioned to 617 mV/dec and 1310 mV/dec at cycles 35 and 80,
496 respectively (**Fig. 5B**). The formation of maghemite increased the inner resistance of the anode
497 material to decrease its reaction rate by forming a resistor-type cyclic voltammogram (**Fig. 5B**),
498 which likely would constrain the BES for extended operating periods.

499 **Impact of carbon corrosion on the duration of the optimum CH_4 production rates**

500 We observed the longest optimum performance periods of three days during the best BES
501 experimental conditions with activated-carbon anodes and soluble-iron addition. We observed and
502 calculated that when the OER was suppressed, accessible carbon-based anode material became the
503 limiting factor to maintain carbon oxidation (**Eq. 1**). We also found that carbon corrosion and the
504 reaction of the released carbon with Fe^{3+} (**Eq. 8**) could explain a stimulation of the CH_4 production
505 rate. On the other hand, carbon corrosion could also impact the CH_4 production rate negatively
506 beyond operating periods of three days due to: **(1)** the exfoliation of carbon material at the cathode,
507 reducing carbon oxidation; and **(2)** the toxicity of a tar-like solution to methanogens.

508 Therefore, we examined carbon corrosion by investigating the surface and the bulk of the anodes
509 with FTIR to track the change of functional groups exhibited at the carbon material. We used the
510 activated-carbon anodes from our abiotic experiments during the measurements of the liquid O_2
511 concentration (no soluble iron was added). Several oxidized functional groups from the initial
512 activated carbon material, such as ketones and phenol groups, were identified by the C=O
513 stretching bond at 1700-1800 cm^{-1} and -OH stretching bonds at 3300-3600 cm^{-1}, respectively (**Fig.**
514 **S8**). The absorbance peak at 2500-3000 cm^{-1} represented the C-H stretching bond of the paraffin
515 oil, which we had added to produce the anodes. The larger absorbance of -OH bonds suggested an
516 alkaline chemical activation of the carbon from the manufacturer. Almost all of the -OH stretches
517 disappeared after five days of anode oxidation. The phenol functional group can act as a catalyst
518 for carbon oxidation and facilitate the CO_2 reaction at the anode. Once the functional group was
519 consumed, the electrode exfoliated in small carbon particles. This exfoliation was also seen during
520 our BES experiment, causing a black electrolyte. Thus, excessive carbon corrosion would
521 eventually stop CH_4 production.

522 While small concentrations of carbon particles in solution might not have a big influence, higher
523 concentrations have shown to influence methanogenesis negatively (Cavalcante et al., 2021).
524 Cavalcante et al. (2021) identified that adding conductive material of carbon particles to a culture
525 of methanogens enhanced methanogenesis. However, inhibition of methanogenesis occurred even
526 at lower carbon material concentrations when the inoculation was performed at a relatively low
527 cell density. In addition, Umetsu et al. (2020) showed that *M. thermautotrophicus* ΔH adsorbed on
528 -OH and -COOH functional groups and prevented hydrogen or mineral uptake, inhibiting
529 methanogenesis. Measures must be taken to reduce the negative effects of carbon corrosion on the
530 anode activity and microbial activity to lengthen the optimum performance period of anode

531 oxidation with sacrificial anodes. The addition of soluble iron, which was shown here to oxidize
532 carbon particles in the electrolyte and improve CH_4 production rates, is one such measure.

533 **DISCUSSION**

534 **Carbon oxidation with sacrificial anodes for single-chamber BES use is ready for research**
535 **purposes within the field of microbial electrosynthesis**

536 Our results showed that implementing carbon oxidation with sacrificial anodes in a single-chamber
537 BES is possible to perform microbial electrosynthesis. We cultivated *M. thermautotrophicus* ΔH
538 with *in-situ* produced H_2 at the cathode under constant pH and temperature conditions to produce
539 CH_4 for an optimum performance period of three days. The growth behavior followed a similar
540 trend for all BESs until the amount of accessible carbon-based anode limited the CH_4 production
541 rates. Our maximum cathode-based geometric CH_4 production rate was already compatible with
542 other studies due to similarly set current densities (Kracke et al., 2020). Further optimizations of
543 our system should increase the geometric CH_4 production rate. With the relatively low current
544 densities of microbial electrosynthesis, our system is already useful for research purposes in the
545 field of microbial electrosynthesis, because the carbon will not become limiting that fast. For
546 example, our collaborators have utilized a single-chamber BES with activated-carbon anodes to
547 grow the acetogen *Sporumusa ovata* successfully, producing acetate within an experimental design
548 of 8 BESs (results not shown). They achieved optimum performance periods of several weeks
549 rather than four days by setting a lower current density than that we had set for CH_4 production.
550 Our work can also inform the earlier studies with a single-chamber BES in the field of perchlorate
551 removal (Zeppilli et al., 2019). We advise the authors to replace the graphite anode materials with
552 activated-carbon anode materials and to add soluble iron to increase the performance.

553 **Is there an opportunity for the industrial application of carbon oxidation with sacrificial**
554 **anodes in BESs for microbial electrosynthesis?**

555 Our system would have a considerably lower theoretical power consumption than membrane-
556 based two-compartment cells due to the lower potential to operate the BES (**Fig. S10**). After
557 optimization of the single-chamber BES and making it continuous, a direct comparison between
558 the production rates and power consumption rates should be performed with a conventional
559 membrane-based cell for microbial electrosynthesis. Another advantage of the single-chamber cell
560 compared to a membrane-based cell would be the lower capital costs due to the absence of ion-
561 exchange membranes, albeit a full techno-economic analysis would be necessary to be conclusive.
562 These advantages make our system a desirable opportunity for scale-up. However, several
563 problems must be overcome.

564 We must prolong the optimum performance period to several months rather than a couple of days.
565 Undoubtedly, carbon corrosion would inhibit the growth of microbial cells during operating
566 periods of several weeks, depending on the current densities. In addition, carbon corrosion would
567 introduce a higher content of -OH, -C=O, and -COOH functional groups, increasing the charge
568 transfer resistance of the carbon material and decreasing the electrochemical performance (Liu et
569 al., 2020). Consequently, the carbon anode decreases its conductivity and current density, while
570 deteriorating. Ideally, carbon corrosion is avoided by efficiently transforming carbon into CO_2 or
571 CO. Studies to mitigate carbon corrosion currently tend to use either expensive catalysts to protect
572 the carbon material or structurally stronger carbon such as graphene or carbon nanotubes (Zhao et
573 al., 2021). In our case, excessive carbon corrosion has to be avoided, and a continuous system
574 rather than our batch system could remove the by-products. Furthermore, mesoporous carbon
575 would enlarge the surface area and the porosity, allowing more reaction sites for carbon oxidation

rather than carbon corrosion. Overall, this proof-of-concept is in its early stages and has ample room for improvement. While we improved one disadvantage of BES by removing the membrane, low conductivities, weak cathode performances, and a sub-optimal reactor setup were still present in our proof-of-concept system. Before industrial application would be possible, several breakthroughs are necessary to overcome these problems.

Acknowledgments

This work was supported by the Deutsche Forschungsgemeinschaft (DFG, German Research Foundation, EBiotech, SPP2240; L.T.A.) – project number 445506379, the Alexander von Humboldt Foundation in the framework of the Alexander von Humboldt Professorship (L.T.A.), and The Novo Nordisk Foundation CO_2 Research Center with grant number NNF21SA0072700 (L.T.A.). L.T.A and A.K. are also grateful to funding from the Deutsche Forschungsgemeinschaft under Germany´s Excellence Strategy – EXC 2124 – 390838134. R.B-G. was supported by an FPI grant (BES-2015-074229) from the Spanish Ministry of Economy and Competitiveness (MINECO) within the research project CTQ2014-53718R. The authors gratefully acknowledge the Tübingen Structural Microscopy Core Facility (Funded by the Federal Ministry of Education and Research (BMBF) and the Baden-Württemberg Ministry of Science as part of the Excellence Strategy of the German Federal and State Governments) for their support and assistance in this work. The authors also thank the German Research Foundation DFG (INST 37/1027-1 FUGG) for financial support provided for the acquisition of the cryogenic focused ion beam scanning electron microscope.

Author Contributions

L.T.A., T.S., and R.B.-G. initiated the work. N.R., T.S., and L.T.A. designed the experiments. N.R. performed the laboratory experiments and analyzed the data. L.T.A. and T.S. supervised the project. N.R. and L.T.A. wrote the manuscript. All edited the paper and approved the final version.

Declaration of interests

The authors declare no conflict of interest.

References

Baek, G., Rossi, R., Saikaly, P.E., and Logan, B.E. (2022). High-rate microbial electrosynthesis using a zero-gap flow cell and vapor-fed anode design. *Water Research* 219**,** 118597. doi: 10.1016/j.watres.2022.118597.

Bard, A.J., and Faulkner, L.R. (2000). *Electrochemical Methods: Fundamentals and Applications, 2nd Edition*. Hoboken, NJ, USA: Wiley.

Bradley, M.J., and Tratnyek, P.G. (2019). Electrochemical characterization of magnetite with agarose-stabilized powder disk electrodes and potentiometric methods. *ACS Earth and Space Chemistry* 3(5)**,** 688-699. doi: 10.1021/acsearthspacechem.8b00200.

Call, D., and Logan, B.E. (2008). Hydrogen production in a single chamber microbial electrolysis cell lacking a membrane. *Environmental Science & Technology* 42(9)**,** 3401-3406. doi: 10.1021/es8001822.

Carmo, M., Fritz, D.L., Mergel, J., and Stolten, D. (2013). A comprehensive review on PEM water electrolysis. *International Journal of Hydrogen Energy* 38(12)**,** 4901-4934. doi: 10.1016/j.ijhydene.2013.01.151.

Cavalcante, W.A., Gehring, T.A., and Zaiat, M. (2021). Stimulation and inhibition of direct interspecies electron transfer mechanisms within methanogenic reactors by adding magnetite and granular actived carbon. *Chemical Engineering Journal* 415**,** 128882. doi: 10.1016/j.cej.2021.128882.

Cheng, S., Xing, D., Call, D.F., and Logan, B.E. (2009). Direct biological conversion of electrical current into methane by electromethanogenesis. *Environmental Science & Technology* 43(10)**,** 3953-3958. doi: 10.1021/es803531g.

Długołęcki, P., Ogonowski, P., Metz, S.J., Saakes, M., Nijmeijer, K., and Wessling, M. (2010). On the resistances of membrane, diffusion boundary layer and double layer in ion exchange membrane transport. *Journal of Membrane Science* 349(1)**,** 369-379. doi: 10.1016/j.memsci.2009.11.069.

Fink, C., Beblawy, S., Enkerlin, A.M., Mühling, L., Angenent, L.T., and Molitor, B. (2021). A shuttle-vector system allows heterologous gene expression in the thermophilic methanogen *Methanothermobacter thermautotrophicus* ΔH. *mBio* 12(6)**,** e02766-02721. doi: doi:10.1128/mBio.02766-21.

Fornero, J.J., Rosenbaum, M., and Angenent, L.T. (2010). Electric power generation from municipal, food, and animal wastewaters using microbial fuel cells. *Electroanalysis* 22(7-8)**,** 832-843. doi: 10.1002/elan.200980011.

Giddings, C.G.S., Nevin, K.P., Woodward, T., Lovley, D.R., and Butler, C.S. (2015). Simplifying microbial electrosynthesis reactor design. *Frontiers in microbiology* 6**,** 468-468. doi: 10.3389/fmicb.2015.00468.

Holubowitch, N.E., Omosebi, A., Gao, X., Landon, J., and Liu, K. (2019). Membrane-free electrochemical deoxygenation of aqueous solutions using symmetric activated carbon electrodes in flow-through cells. *Electrochimica Acta* 297**,** 163-172. doi: 10.1016/j.electacta.2018.11.106.

Jourdin, L., Raes, S.M.T., Buisman, C.J.N., and Strik, D.P.B.T.B. (2018). Critical biofilm growth throughout unmodified carbon felts allows continuous bioelectrochemical chain elongation from CO_2 up to caproate at high current density. *Frontiers in Energy Research* 6(7). doi: 10.3389/fenrg.2018.00007.

Ju, H., Badwal, S., and Giddey, S. (2018). A comprehensive review of carbon and hydrocarbon assisted water electrolysis for hydrogen production. *Applied Energy* 231**,** 502-533. doi: 10.1016/j.apenergy.2018.09.125.

Kiener, A., and Leisinger, T. (1983). Oxygen sensitivity of methanogenic bacteria. *Systematic and Applied Microbiology* 4(3)**,** 305-312. doi: 10.1016/s0723-2020(83)80017-4.

Kim, K.J., Fane, A.G., Nystrom, M., Pihlajamaki, A., Bowen, W.R., and Mukhtar, H. (1996). Evaluation of electroosmosis and streaming potential for measurement of electric charges of polymeric membranes. *Journal of Membrane Science* 116(2)**,** 149-159. doi: 10.1016/0376-7388(96)00038-5.

Kracke, F., Deutzmann, J.S., Gu, W., and Spormann, A.M. (2020). In situ electrochemical H_2 production for efficient and stable power-to-gas electromethanogenesis. *Green Chemistry* 22(18)**,** 6194-6203. doi: 10.1039/D0GC01894E.

Kumar, M., Sandipam, S., Puri, S.K., Ramakumar, S.S.V., Diels, L., Bouwan, L., et al. (2020). *Membrane-less reactor and biotransformation of carbon dioxide*. European Patent No EP3831983.

Lai, A., Aulenta, F., Mingazzini, M., Palumbo, M.T., Papini, M.P., Verdini, R., et al. (2017). Bioelectrochemical approach for reductive and oxidative dechlorination of chlorinated aliphatic hydrocarbons (CAHs). *Chemosphere* 169**,** 351-360. doi: 10.1016/j.chemosphere.2016.11.072.

Liu, X., Xu, W., Zheng, D., Li, Z., Zeng, Y., and Lu, X. (2020). Carbon cloth as an advanced electrode material for supercapacitors: progress and challenges. *Journal of Materials Chemistry A* 8(35)**,** 17938-17950. doi: 10.1039/D0TA03463K.

Lovley, D.R., and Nevin, K.P. (2012). *Microbial production of multi-carbon chemicals and fuels from water and carbon dioxide using electric current*. USA Patent No 9,856,449.

Mano, N., Mao, F., and Heller, A. (2004). A miniature membrane-less biofuel cell operating at +0.60 V under physiological conditions. *ChemBioChem* 5(12)**,** 1703-1705. doi: 10.1002/cbic.200400275.

Martin, M.R., Fornero, J.J., Stark, R., Mets, L., and Angenent, L.T. (2013). A Single-culture bioprocess of *Methanothermobacter thermautotrophicus* to upgrade digester biogas by CO_2-to-CH_4 conversion with H_2. *Archaea* 2013. doi: 10.1155/2013/157529.

Nevin, K.P., Woodard, T.L., Franks, A.E., Summers, Z.M., and Lovley, D.R. (2010). Microbial electrosynthesis: Feeding microbes electricity to convert carbon dioxide and water to multicarbon extracellular organic compounds. *mBio* 1(2)**,** e00103-00110. doi: 10.1128/mBio.00103-10.

Rabaey, K., and Rozendal, R.A. (2010). Microbial electrosynthesis -- revisiting the electrical route for microbial production. *Nature Reviews Microbiology* 8(10)**,** 706-716. doi: 10.1038/nrmicro2422.

Roberts, J.J.P., Westgard, J.A., Cooper, L.M., and Murray, R.W. (2014). Solution voltammetry of 4 nm magnetite iron oxide nanoparticles. *Journal of the American Chemical Society* 136(30)**,** 10783-10789. doi: 10.1021/ja505562p.

Rozendal, R.A., Hamelers, H.V.M., and Buisman, C.J.N. (2006). Effects of membrane cation transport on pH and microbial fuel cell performance. *Environmental Science & Technology* 40(17)**,** 5206-5211. doi: 10.1021/es060387r.

Schill, N., van Gulik, W.M., Voisard, D., and von Stockar, U. (1996). Continuous cultures limited by a gaseous substrate: Development of a simple, unstructured mathematical

model and experimental verification with *Methanobacterium thermoautotrophicum*. *Biotechnol Bioeng* 51(6), 645-658. doi: 10.1002/(sici)1097-0290(19960920).

Sorwat, J., Mellage, A., Kappler, A., and Byrne, J.M. (2020). Immobilizing magnetite onto quartz sand for chromium remediation. *Journal of Hazardous Materials* 400, 123139. doi: 10.1016/j.jhazmat.2020.123139.

Stookey, L.L. (1970). Ferrozine---a new spectrophotometric reagent for iron. *Analytical Chemistry* 42(7), 779-781. doi: 10.1021/ac60289a016.

Sun, T., Levin, B.D.A., Guzman, J.J.L., Enders, A., Muller, D.A., Angenent, L.T., et al. (2017). Rapid electron transfer by the carbon matrix in natural pyrogenic carbon. *Nature Communications* 8(1), 14873. doi: 10.1038/ncomms14873.

Tremblay, P.-L., Angenent, L.T., and Zhang, T. (2017). Extracellular electron uptake: Among autotrophs and mediated by surfaces. *Trends in Biotechnology* 35(4), 360-371. doi: 10.1016/j.tibtech.2016.10.004.

Umetsu, M., Sunouchi, T., Fukuda, Y., Takahashi, H., and Tada, C. (2020). Functional group distribution of the carrier surface influences adhesion of *Methanothermobacter thermautotrophicus*. *Archaea* 2020, 9432803. doi: 10.1155/2020/9432803.

Yee, R.S.L., Rozendal, R.A., Zhang, K., and Ladewig, B.P. (2012). Cost effective cation exchange membranes: A review. *Chemical Engineering Research and Design* 90(7), 950-959. doi: 10.1016/j.cherd.2011.10.015.

Yi, Y., Weinberg, G., Prenzel, M., Greiner, M., Heumann, S., Becker, S., et al. (2017). Electrochemical corrosion of a glassy carbon electrode. *Catalysis Today* 295, 32-40. doi: 10.1016/j.cattod.2017.07.013.

Yin, R., Zhao, Y., Lu, S., Wang, H., Cao, W., and Fan, Q. (2009). Electrocatalytic oxidation of coal on Ti-supported metal oxides coupled with liquid catalysts for H2 production. *Electrochimica Acta* 55(1), 46-51. doi: 10.1016/j.electacta.2009.07.090.

Zeppilli, M., Dell'Armi, E., Cristiani, L., Petrangeli Papini, M., and Majone, M. (2019). Reductive/oxidative sequential bioelectrochemical process for perchloroethylene removal. *Water* 11(12), 2579.

Zhang, Y., Li, F., Liu, X., Lu, J., and Zhang, G. (2017). Promoting influence of activated carbon used in carbon paste electrode on platinum nanoparticles efficiency in methanol electrooxidation. *Electrochimica Acta* 242, 165-172. doi: 10.1016/j.electacta.2017.05.020.

Zhao, J., Tu, Z., and Chan, S.H. (2021). Carbon corrosion mechanism and mitigation strategies in a proton exchange membrane fuel cell (PEMFC): A review. *Journal of Power Sources* 488, 229434. doi: 10.1016/j.jpowsour.2020.229434.